Available online at www.sciencedirect.com
SCIENCE DIRECT®
Energy and Buildings 36 (2004) 567–578
ENERGY and BUILDINGS
www.elsevier.com/locate/enbuild

Development of a thermally activated ceiling panel with PCM for application in lightweight and retrofitted buildings

Markus Koschenz*, Beat Lehmann

Laboratory for Energy Systems/Building Equipment, Swiss Federal Laboratories for Materials Testing and Research (EMPA), Ueberlandstrasse 129, CH-8600 Duebendorf, Switzerland

Received 1 June 2003; received in revised form 17 December 2003; accepted 10 January 2004

Abstract

This paper describes the development of a thermally activated ceiling panel for incorporation in lightweight and retrofitted buildings. The system allows use of renewable energy sources for the heating and cooling of office and industrial buildings. The design for the new ceiling panel exploits the properties of the phase change material (PCM) paraffin. Its high thermal storage capacity during phase change—up to 300 Wh/(m^2 day)—enables the overall panel thickness to be limited to a mere 5 cm. Active control of the thermal storage is achieved by means of an integrated water capillary tube system. The research project also included the development of a numerical model for computation of the thermal behavior of wall and ceiling systems incorporating PCMs. Simulation calculations were performed to determine the necessary thermal properties of the ceiling panels and specify requirements for the materials to be used. Laboratory tests were performed to verify the system's performance and a pilot application is soon to be tried out in practice.

Keywords: Latent heat thermal energy storage; Thermally activated building systems; Cooling of buildings with renewable energy sources; Phase change material; PCM

1. Introduction

Even today, refurbishment schemes account for a significant proportion of construction activity in the commercial sector (office and industrial buildings), and the increasing shortage of development sites in urban centers looks set to consolidate this trend in future. Any breakthrough in the application of sustainable energy systems to both retrofit and new-build schemes will depend on a wider use of renewable energy sources in the operation of building technologies, particularly heating and cooling.

Both the enhanced technical installation requirements of workplaces and the increased use of fully glazed facades favored by contemporary architecture have forced up the internal and external thermal loads in modern office buildings. As a result, such facilities now require cooling for much of the year. To prevent an unacceptable rise in the indoor temperature, thermal gains have to be removed from the building interior. Conventional systems rely on ventilation or chilled ceiling panels. While, at present, compression refrigerators generally provide the necessary cooling energy, forward-looking solutions will increasingly seek to exploit natural cooling sources. These may involve the use of ground-coupled heat exchangers, groundwater or outside air. However, these renewable energy sources are frequently unable to provide the necessary heating or cooling power or the energy supply is non-concurrent in time with demand. Though outside air is universally available, for instance, its temperature in summer is usually only low enough at night to serve as a cooling medium.

A suitable thermal storage is therefore needed to overcome this time lag. Standard water systems may be discounted due to the excessive plant size and space allocation needed to store sufficient energy for daily needs. Thermally activated building systems (tabs) [1], which use the building structure as a heat sink, are a more recent approach. Heat gains during the day are stored in solid floors and slabs, which are then recooled at an appropriate time by means of a water pipe system—the extracted energy being rejected to the outside, e.g. via cooling tower. This system lends itself to incorporation in new buildings, where provision can be made in the design for casting the necessary pipework into the floor slabs. The retrofitting of pipes as part of an alteration scheme, on the other hand, is problematic. Moreover, retrofitted service installations like air ducts are commonly

* Corresponding author. Tel.: +41-1-823-4175; fax: +41-1-823-4020.
E-mail address: markus.koschenz@empa.ch (M. Koschenz).

0378-7788/$ – see front matter © 2004 Elsevier B.V. All rights reserved.
doi:10.1016/j.enbuild.2004.01.029

Nomenclature

a	thermal diffusivity (m^2/s)
Bi	Biot number
c	specific heat capacity (J/kg K)
dm	melting range (K)
e	enthalpy (J/kg)
h	convective heat transfer coefficient (W/m^2 K)
L	latent heat of fusion (J/kg)
M	modulus
St	Stefan number
t	time (s)
λ	conductivity (W/mK)
Θ	parameter of time
ρ	density (kg/m^3)
ϑ	temperature (°C)
x	space coordinate (m)
X	interface location (m)

Indices

b	boundary
i	node number in space
in	initial
l	liquid
m	melting
n	node number in time
s	solid
su	supply
tubes	capillary tube system
0	surface
1	side 1
2	side 2
∞	fluid

located above a suspended ceiling, which prevents the transfer of heat from its source to the structural elements.

This explains the present lack of thermal storage units suitable for local installation in altered or refurbished buildings, which permit use of renewable energy sources for heating and cooling.

This report outlines the development of a thermally activated ceiling panel by means of model-based computational simulations and laboratory tests, and describes the prototype modules due to be tested in a pilot building.

2. Concept for a new ceiling panel

2.1. Requirements and principle

As mentioned above, the aim was to design a thermally activated ceiling panel permitting the use of alternative energy sources. An initial priority was to achieve a thermal storage capacity approximately equal to the heat gains within the space during the daily cycle. Furthermore, due to the particular constraints imposed by alteration and refurbishment schemes, the thermal storage had to be assembled afterwards in the building interior while occupying minimum space.

The above requirements coupled with the fact that ceilings offer the most appropriate location in buildings for this type of installation prompted the choice of ceiling panels as the thermal storage early in the concept design phase. The key issue was how to provide adequate thermal mass within a small panel thickness. Phase change materials (PCMs) emerged as the prime option as the phase change undergone by these materials allows storage and release of substantial quantities of heating or cooling energy. The PCM in the ceiling panels melts during the daytime upon exposure to the thermal loads and freezes overnight when cooled by means of an integrated water pipe system. The interim storage of thermal energy in the PCM damped the temperature amplitude within the building while enabling the heat rejection process to be non-concurrent with heat gain.

2.2. Realization of the concept

An investigation into the different ways of incorporating PCM in the ceiling panels revealed difficulties in the use of pure PCM. Such an assembly would necessitate stringent fire precautions to prevent the escape of liquid paraffin. Instead, microencapsulated paraffin bedded in a suitable carrier material—in this case gypsum—was selected. Passive applications of this technology in composite wall systems and plaster coats have recently been investigated [2,3]. Through the gypsum, the PCM is encased in a stable structure while the constitutional water contained in the gypsum retards flame spread in the event of fire.

The overall concept for the ceiling panels adopts the following arrangement (see Fig. 1): a sheet steel tray serves as a container for the PCM/gypsum composite while providing the panels with the required mechanical stability. A mix comprising microencapsulated PCM and gypsum is poured into the tray. Active control of the thermal mass is achieved by incorporation of a capillary water tube system in the

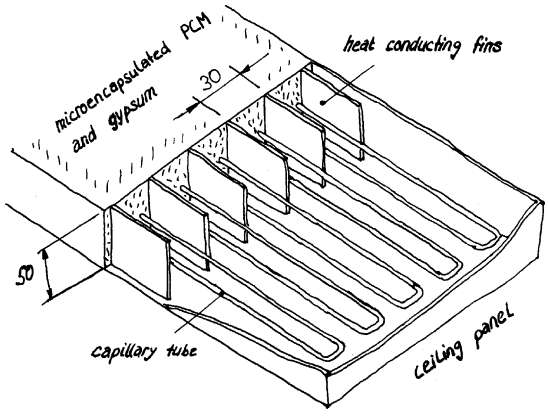

Fig. 1. Schematic drawing of thermally activated ceiling panel with PCM.

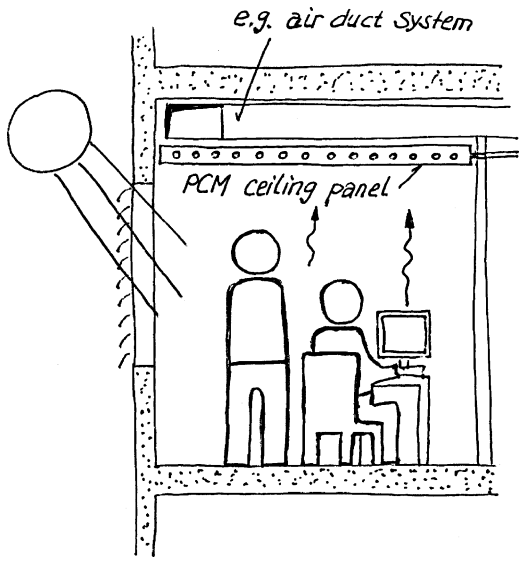

Fig. 2. Installation of ceiling panels in building interior as suspended ceiling.

gypsum compound. If required, thermal conduction in the composite may be improved by the inclusion of aluminum fins. While the panel is primarily designed for ceiling installation, fitting to walls is equally straightforward (Fig. 2). An international patent application has been filed for the system.

3. Method

To minimize effort, development work was as far as possible computer-based. This allowed definition of the thermal and material-related requirements for the ceiling panels together with an approximate sizing of the system. For the purposes of computational simulation, a special thermal model was developed which, through integration in the TRNSYS building and system simulation environment [4], allowed similar calculations to be performed for real buildings with integrated PCM ceiling panels. The laboratory tests performed concurrently with the calculations prompted a number of optimizations while supplying empirical data to validate the concept and thermal design of the PCM ceiling panels. Prototype modules installed in a pilot building will provide a further check on the practicability of the solution. The following sections offer a detailed description of the individual development stages.

4. Properties of phase change materials

4.1. General properties of PCMs

In addition to the sensible heat of PCMs, the latent heat stored during melting and freezing offers particular benefits. The key asset of PCMs is their high thermal storage capacity, which, for unit thickness, is many times that of conventional building materials like concrete, etc.

Common PCMs include paraffins, salt hydrates, alcohols, fatty acids, and synthetic materials. By virtue of their chemical composition, the wax-like paraffins exhibit high cycle stability, low reactivity, low hysteresis and are classed as non-toxic–properties that make them ideal for use in building applications. Moreover, their thermal properties, specifically the melting point range, may be substantially adjusted by blending pure materials. The main drawback of paraffins, a by-product of petroleum distillation, is their combustibility.

Fig. 3 shows the general behavior of the two most important PCM groups in terms of melting point and range, specific heat and enthalpy. As can be seen, inorganic PCMs, such as salt hydrates, exhibit a relatively narrow melting range, and therefore, remain at a constant temperature during the entire melting or freezing process. Organic PCMs such as paraffins, by contrast, display a wider melting range (“mushy region”) that varies according to purity, together with an increased rise in thermal capacity within this range. Hysteresis, as a measure of the divergence of melting and freezing curves, is a further characteristic feature, particularly marked in the case of inorganic PCMs.

4.2. Physical properties of paraffins

So-called normal paraffins are commonly used in thermal applications. These comprise long-chain molecules of the general formula C_nH_{2n+2}. The value of n for paraffins with a melting point between 18 and 90 °C ranges from 16 to 50—the longer the molecular chain or greater the molecular mass, the higher the melting point.

Inside room temperatures of between 21 and 28 °C, and thus, surface temperatures of 21–24 °C, are a prerequisite for thermal comfort in buildings. Hence, to fully exploit the phase change of PCMs, the melting range of the selected PCM must also lie within this region. This basic requirement is met by the paraffins listed in Table 1, [5], or mixtures of these substances.

The listed values of latent heat are valid for chemically pure substances and all their occuring melting ranges. Technical grade materials show clearly lower values depending on their purity. According to the planned operating range may be only a certain part of the latent heat will be usable depending on the distribution of the different melting ranges. In addition, the mixing of different types of paraffin to adjust the melting point further reduces the useful latent heat of fusion as this is spread over a bigger number of melting ranges in the mix.

As described in Section 2.2, the ceiling panels incorporate paraffin in microencapsulated form. This ensures that minute quantities of the phase change material will remain permanently enclosed in the capsules even when subjected to frequent cyclical loads, what has been determined as a problem with PCM-impregnated wallboards. Some 10 μm in diameter, the plastics capsules are manufactured from a

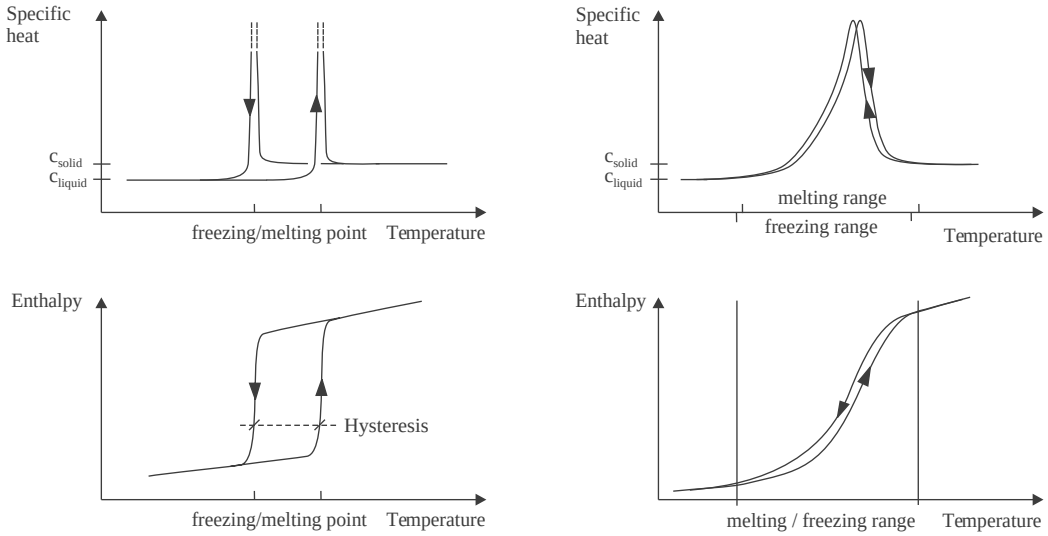

Fig. 3. General behavior of inorganic and organic phase change materials in terms of specific heat and enthalpy.

Table 1
Physical properties of pure paraffins with melting points between 18 and 28 °C

Paraffin	Molecular formula	Melting point (°C)	Latent heat of fusion (J/kg)	Specific heat solid (J/kgK)	Specific heat liquid (J/kgK)	Thermal conductivity (W/mK)	Density (kg/m^3)
Hexadecane	CH_3–$(CH_2)_{14}$–CH_3	18	236,000	1650	2100	0.17	780
Heptadecane	CH_3–$(CH_2)_{15}$–CH_3	22	214,000			to	780
Octadecane	CH_3–$(CH_2)_{16}$–CH_3	28	244,000	1750	2100	0.26	780

water/paraffin solution by means of in situ synthesis. BASF is conducting extensive research into micro-encapsulation [6] and produced capsule dispersions tailored to the needs of the project. Owing to the volume losses through the capsule wall material (20–25% by volume) and the air spaces between the capsules (5% by volume) the latent heat of fusion of microencapsulatet paraffin is reduced compared to the basic material being encapsulated. As an illustration the latent heat of fusion of the finally used Heptadecane is—for its various forms—listet in Table 2.

4.3. Physical properties of PCM ceiling panel

Throughout the development process, the material composition of the ceiling panels was optimized and adjusted to suit the specific environmental requirements (see Section 6). Table 3 and Fig. 4 show the overall properties of the final version of the ceiling panel. These also formed the basis for the comparison of the model against the laboratory tests.

Table 2
Latent heat of fusion of heptadecane in its various forms

Form	Latent heat of fusion (J/kg)
Pure heptadecane, all melting ranges	214,000
Pure heptadecane, melting peak at 20 °C only	177,000
Technical grade heptadecane as used in the project, melting peak at 20 °C only	148,300
Technical grade heptadecane, after micro-encapsulation	110,000

Table 3
Physical properties of the composit ceiling panel

Quantity	Value
Density (kg/m^3)	1030
Thermal conductivity (W/mK)	1.15
Amount of micro-encapsulated PCM (kg/m^2)	13.3
Melting peak (°C)	22

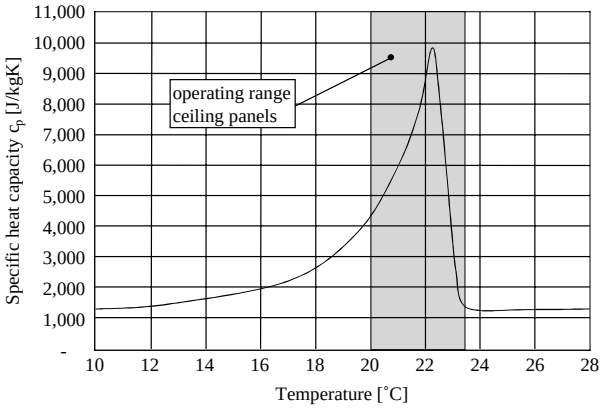

Fig. 4. Specific heat capacity c_p of PCM ceiling panel after optimization.

5. Thermal modeling of wall systems with PCM

To assist the computer-based development of the ceiling panel, a numerical model was specially devised to simulate the processes taking place during phase change. Integration

of the model in the TRNSYS building and system simulation program [4] also allowed investigation of the behavior of real buildings with PCM ceiling panels.

5.1. Theoretical background

5.1.1. Basic equation

Background literature identifies two general methods for dealing with solid–liquid phase change heat transfer as introduced in Section 4.1: (1) where the substance has a discrete phase change temperature and a sharply defined interface (inorganics, e.g. salt hydrates) and (2) where the substance undergoes phase change over a range of temperatures, with a mushy region existing between the solid and liquid phases (organics, e.g. paraffin). As paraffin is the PCM investigated in this study, the focus will be on the second method. For continuous phase change materials a modeling approach was developed by [7]. Yet, as shown in Section 5.2.2, considered in the context of the Stefan problem, the model also provides good results for small mushy regions.

First, the energy conservation equation is formulated:

$$\rho\frac{\partial e}{\partial t}+\frac{\partial}{\partial x}\left(-\lambda\,(\vartheta)\,\frac{\partial\vartheta}{\partial x}\right)=0 \tag{1}$$

In Eq. (1), density ρ is considered as constant whereas conductivity λ is a function of temperature. By performing the inner derivative on Eq. (1) and applying the product law of calculus to both $\partial e/\partial t$ and $\partial\lambda/\partial x$ we arrive at:

$$\rho\frac{\mathrm{d}e}{\mathrm{d}\vartheta}\frac{\partial\vartheta}{\partial t}-\lambda\,(\vartheta)\,\frac{\partial^2\vartheta}{\partial x^2}-\frac{\mathrm{d}\lambda}{\mathrm{d}\vartheta}\left(\frac{\partial\vartheta}{\partial x}\right)^2=0 \tag{2}$$

The enthalpy derivative $\mathrm{d}e/\mathrm{d}\vartheta$ describes the specific heat:

$$c(\vartheta)=\frac{\mathrm{d}e}{\mathrm{d}\vartheta} \tag{3}$$

and, assuming constant density, thermal diffusivity is defined as follows:

$$a(\vartheta)=\frac{1}{\rho}\frac{\lambda(\vartheta)}{c(\vartheta)} \tag{4}$$

By applying Eqs. (3) and (4) to (2), we arrive at:

$$\frac{\partial\vartheta}{\partial t}=a(\vartheta)\left[\frac{\partial^2\vartheta}{\partial x^2}+\frac{1}{\lambda(\vartheta)}\frac{\mathrm{d}\lambda}{\mathrm{d}\vartheta}\left(\frac{\partial\vartheta}{\partial x}\right)^2\right] \tag{5}$$

Assuming constant conductivity λ, an issue given further consideration below, Eq. (5) may be simplified to:

$$\frac{\partial\vartheta}{\partial t}=a(\vartheta)\frac{\partial^2\vartheta}{\partial x^2} \tag{6}$$

5.1.2. Numerical method

Explicit and approximate solutions for PCM processes are obtained only for simple problems with specific boundary conditions. As most realistic phase change processes do not fall into this category, the mathematical problems modeling such processes may only be solved numerically.

In our study we use the finite-difference (FD) method to numerically approximate the partial differential equations (PDE) similar to the investigations in [8]. All PDE terms in Eq. (6) will be replaced by algebraic equations at discrete points in the space–time domain. The grid points are referenced by an index i for the space coordinate and n for the time coordinate.

The derivative $\partial\vartheta/\partial t$ in Eq. (6), can be formulated by an algebraic equation through a first-order forward difference expression:

$$\left(\frac{\partial\vartheta}{\partial t}\right)_i^n=\frac{\vartheta_i^{n+1}-\vartheta_i^n}{\Delta t}+\mathrm{O}(\Delta t) \tag{7}$$

The second derivative $\partial^2\vartheta/\partial x^2$ can be formulated for the grid point i at time $n+\Theta$ by a second-order central difference expression:

$$\left(\frac{\partial^2\vartheta}{\partial x^2}\right)_i^{n+\Theta}=\frac{\vartheta_{i+1}^{n+\Theta}-2\vartheta_i^{n+\Theta}+\vartheta_{i-1}^{n+\Theta}}{\Delta x^2}+\mathrm{O}(\Delta x)^2 \tag{8}$$

where $0\le\Theta\le 1$. The usual choices are $\Theta=0$, 1/2, or 1 and this will be discussed later.

Now we replace the left-hand side of Eq. (6) with the algebraic Eq. (7) and the right-hand side with Eq. (8). Finally we obtain the general finite-difference scheme for Eq. (6)

$$\vartheta_i^{n+1}=\vartheta_i^n+M_i^n\Big[(1-\Theta)(\vartheta_{i+1}^n-2\vartheta_i^n+\vartheta_{i-1}^n)+\Theta(\vartheta_{i+1}^{n+1}-2\vartheta_i^{n+1}+\vartheta_{i-1}^{n+1})\Big] \tag{9}$$

where the modulus is defined as:

$$M_i^n=a(\vartheta_i^n)\frac{\Delta t}{\Delta x^2} \tag{10}$$

If we set $\Theta=0$, we obtain the explicit calculation method. The temperature at time $n+1$ can be calculated directly from the known temperatures at time n. With $\Theta=1/2$, we obtain the Crank–Nicolson method and with $\Theta=1$ the fully implicit method. The temperature variation for the three different schemes is shown in Fig. 5. Choosing the parameter

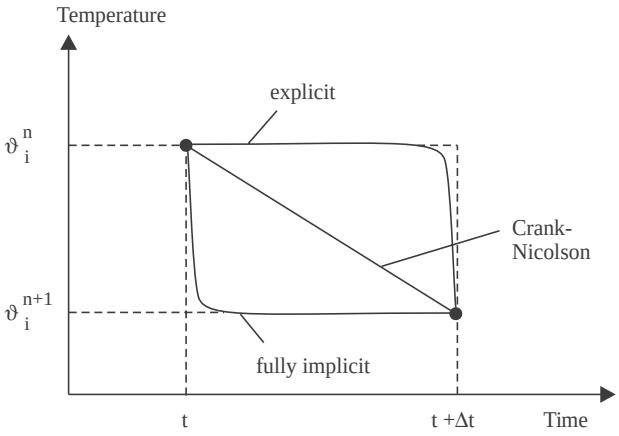

Fig. 5. Variation of temperature with time for three different schemes [9].

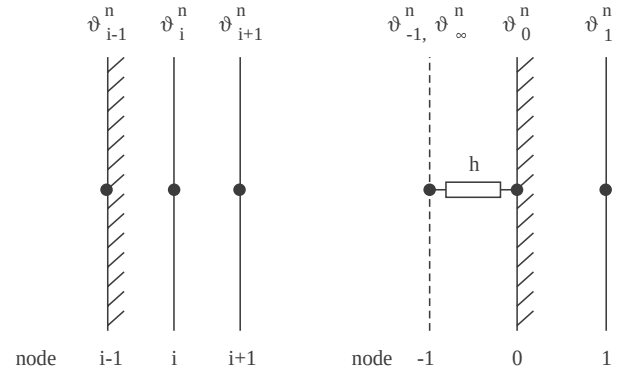

Fig. 6. Three-node example for imposed temperatures (left) or convective boundary conditions (right).

$\Theta > 0$, results in a system of simultaneous equations for the unknown temperatures at ϑ_i^{n+1}. The advantage of the implicit methods lies in their higher numerical stability as discussed in the following section.

5.1.3. Heuristic arguments of stability

In numerical solutions to finite-difference equations, round-off errors are introduced during calculations. The mathematical analysis of stability is concerned with the examination of the growth of errors while computations are being performed. Various rigorous mathematical methods, such as the Fourier or Neumann method, exist to analyze stability criteria for finite-difference equations. However, a number of more straightforward heuristic arguments may serve to define stability criteria.

5.1.4. Imposed temperatures

First we will study the case of known temperatures at the boundary nodes.

Let us assume the following boundary conditions where ϑ_b is a fixed temperature at node $i-1$ and $i+1$ respectively and ϑ_{in} is the initial temperature of node i, which has a lower value than ϑ_b (Fig. 6, left side).

$$\vartheta_{i-1}^n = \vartheta_{i+1}^n = \vartheta_{i-1}^{n+1} = \vartheta_{i+1}^{n+1} = \vartheta_b$$

$$\vartheta_i^n = \vartheta_{in}$$

The physical situation requires that the unknown temperature ϑ_i^{n+1} cannot exceed the fixed boundary temperature ϑ_b. We therefore, propose the following condition:

$$\vartheta_i^{n+1} \leq \vartheta_b$$

Now we put Eq. (10) into Eq. (9) and rearrange for modulus M_i^n:

$$M_i^n = \frac{\vartheta_i^{n+1} - \vartheta_i^n}{(1-\Theta)\cdot(\vartheta_{i+1}^n - 2\cdot\vartheta_i^n + \vartheta_{i-1}^n) + \Theta\cdot(\vartheta_{i+1}^{n+1} - 2\cdot\vartheta_i^{n+1} + \vartheta_{i-1}^{n+1})} \quad (11)$$

Given the specific boundary conditions defined above, we obtain the general stability criteria:

$$M_i^n \leq \frac{1}{2(1-\Theta)} \quad (12)$$

which for the explicit calculation scheme with $\Theta = 0$ is:

$$M_i^n \leq \tfrac{1}{2} \quad (13)$$

for Crank–Nicolson with $\Theta = 1/2$:

$$M_i^n \leq 1 \quad (14)$$

and for the implicit calculation scheme with $\Theta = 1$:

$$M_i^n \leq \infty \quad (15)$$

The accuracy for the explicit as well as for the implicit calculation scheme is of first order in time $O(\Delta t)$ where the Crank–Nicolson scheme is of second order $O(\Delta t^2)$ [10]. The advantage of the implicit schemes lies in their superior stability properties. Indeed, Eq. (9) with $1/2 \leq \Theta \leq 1$ is known to be unconditionally stable, thus imposing no restrictions on the time step. As described in [9], an inexperienced user often interpretes this to imply that a physically realistic solution will result no matter how large the time step, and such a user is, therefore, surprised to encounter oscillatory solutions. The "stability" in a mathematical sense simply ensures that these oscillations will eventually die out, but it does not guarantee physically plausible solutions. Some examples of unrealistic solutions given by the Crank–Nicolson scheme can be found in [11].

To obtain stability in the whole calculation domain the modulus has to satisfy the following condition:

$$M \leq \max\{a_i^n\}\frac{\Delta t}{\Delta x^2} \quad (16)$$

Using Eqs. (12) and (16), the relation between the time-step Δt and the grid-spacing Δx is given by:

$$\frac{\Delta t}{\Delta x^2} \leq \frac{1}{2(1-\Theta)\max\{a_i^n\}} \quad (17)$$

5.1.5. Convective boundary conditions

The convective heat transfer at the surface is given as (Fig. 6, right side):

$$-\lambda\frac{\partial\vartheta}{\partial x} + h\vartheta_0 = h\vartheta_\infty \quad (18)$$

where ϑ_0^n is the unknown temperature.

The algebraic equation for the boundary surface node ϑ_0^{n+1}can be calculated in a similar way as described for Eq. (9). The boundary condition Eq. (18) is discretized by central second-order differencing. To apply central differencing, we consider a fictitious node "−1" at a fictitious temperature ϑ_{-1}^n obtained by extending the region by Δx to the left, as illustrated in Fig. 6:

$$-\lambda\frac{\vartheta_1^n - \vartheta_{-1}^n}{2\Delta x} + h\vartheta_0^n = h\vartheta_\infty^n \quad (19)$$

Table 4
Modulus based on Eq. (22) with $\Theta = 0$ for different materials calculated using typical values for building applications

Material	λ (W/mK)	Δx (m)	h (W/m^{2}K)	Bi	M
Paraffin	0.20	0.005	10	0.25	0.40
Concrete	1.80	0.005	10	0.03	0.49
Insulation	0.05	0.005	10	1.00	0.25

In the next step, Eq. (9) is evaluated for $i = 0$ and the resulting fictitious temperature ϑ^n_{-1} is eliminated by applying the equation obtained by discretizing the boundary condition Eq. (18) as shown in Eq. (19). Finally, the following second-order difference equation for the convective boundary conditions is obtained:

$$\vartheta_0^{n+1} = \vartheta_0^n + 2M_i^n\{(1-\Theta)[\vartheta_1^n - (1+Bi)\vartheta_0^n + Bi\vartheta_\infty^n] + \Theta[\vartheta_1^{n+1} - (1+Bi)\vartheta_0^{n+1} + Bi\vartheta_\infty^{n+1}]\} \quad (20)$$

with the Biot-number:

$$Bi = \frac{h\Delta x}{\lambda} \quad (21)$$

If we evaluate Eq. (20) with the same boundary conditions chosen for imposed temperatures we obtain for the modulus:

$$M_0^n \leq \frac{1}{2(1-\Theta)(1+Bi)} \quad (22)$$

If we compare Eq. (12) with Eq. (22), we clearly see that the stability criteria for convective heat transfer are more restrictive than those for imposed temperatures.

As shown in Table 4, the stability criteria for both paraffin and concrete, with a convective heat transfer coefficient $h = 10\,\mathrm{W/m^2K}$ normally used for building applications, are close to $M = 1/2$. For insulation materials the modulus is approximately halved.

5.2. Modeling

5.2.1. Model for one-dimensional wall system with PCM

The theoretical model described in the previous section was transferred to a program routine and integrated into TRNSYS [4]. To reach a maximum of accuracy simultaneously to an acceptable time step the Crank–Nicolson method was used as calculation scheme. The coupling of the new model to the building type 56 was carried out by convective boundary conditions as well as heat flows specified as wall gains. A schematic representation of the model is shown in Fig. 7. It allows computation of the thermal behavior of one-dimensional wall systems comprising common construction materials such as concrete, wood or insulation in conjunction with PCM. The material properties of the single layers are entered as mathematical functions or as measured data, especially in the case of PCM thermal capacity. A water piping system for cooling and heating purposes can be coupled to any node of the model.

5.2.2. Testing of model

The numerical model from Eq. (9) may be tested against the Neumann analytical solution for the freezing case [12]. The idea to use the Stefan problem as a benchmark for the model based on the assumption that the behaviour of the real material Heptadecane with a mushy region of a few degrees converges to the Neumann solution for smaller melting ranges.

For the conditions $a_s = a_l = a$ and $c_s = c_l = c$ the interface location $X(t)$ is calculated as:

$$X(t) = 2\xi\sqrt{at} \quad (23)$$

where ξ is the solution of the transcendental equation:

$$\frac{St}{\xi\sqrt{\pi}}\exp(-\xi^2)\left[\frac{1}{erf(\xi)} - \frac{1}{erfc(\xi)}\right] = 0 \quad (24)$$

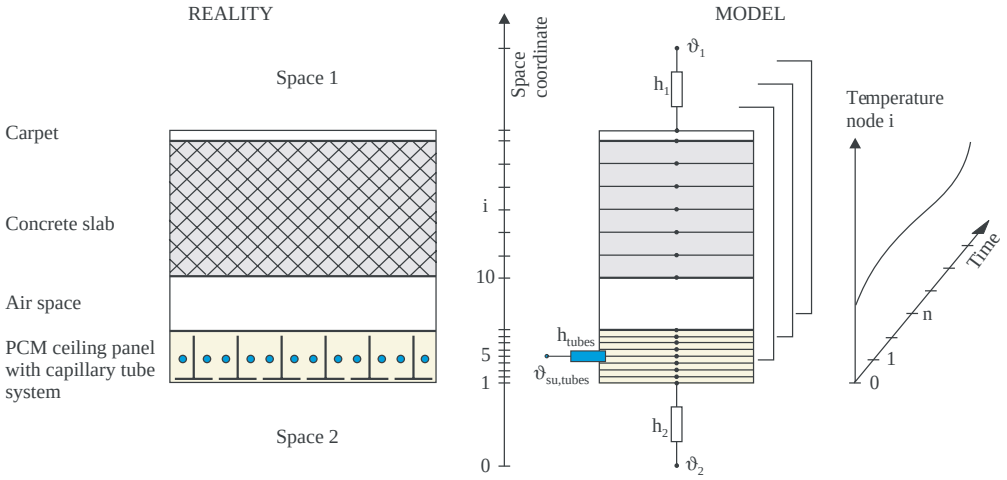

Fig. 7. Model for computation of wall system with integrated PCM layers.

Table 5
Initial boundary conditions and material properties chosen for comparison of the model against the Neumann solution

Quantity	Value
ϑ_m (°C)	22
ϑ_s (°C)	17
ϑ_l (°C)	27
λ (W/mK)	0.20
ρ (kg/m^3)	780
c (J/kgK)	2,000
L (J/kg)	148,300
Grid spacing (m)	0.001/0.002

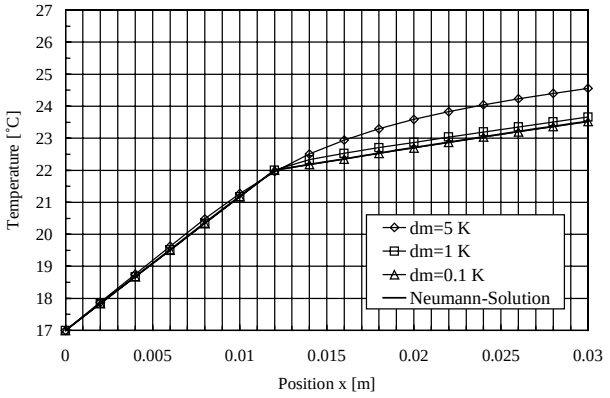

Fig. 8. Temperature distribution in the material at $t = 10,800$ s for different melting ranges and Neumann solution for this case.

The Stefan number St is defined as:

$$St = \frac{c(\vartheta_m - \vartheta_s)}{L} \quad (25)$$

With the conditions specified in Table 5, Eq. (24) gives:

$$\xi = 0.1608$$

Fig. 8 shows the temperature distribution in the material at $t = 10{,}800$ s with an interface location at $X(t) = 0.012$ m. As expected the simulation results converge to the Neumann solution for smaller melting ranges. A material with a melting range lower than 1 K shows almost the behavior of a substance with a discrete phase change.

The time dependent interface location of the Neumann solution $X(t)$ is compared against the model with a mushy region of 0.1 K and a grid spacing of 1 and 2 mm. As shown in (Fig. 9), the difference between the calculated interface location and the Neumann solution is mainly influenced by the space grid width.

6. Thermal design of ceiling panel

6.1. Thermal requirements for ceiling panel

The ceiling panels were to be designed for use in standard office buildings with high thermal loads. To reach appropriate thermal comfort the room temperature should be

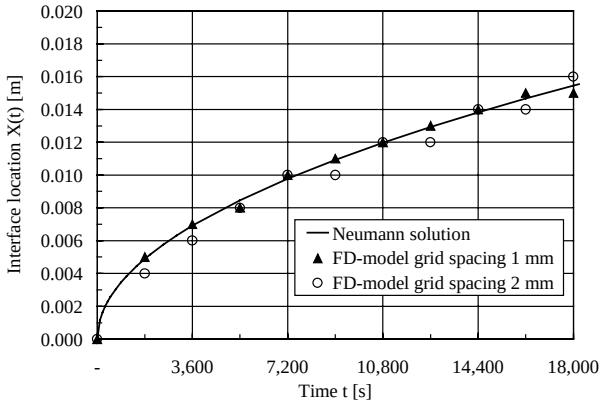

Fig. 9. Interface location $X(t)$ during freezing process.

in the range between 21 and 28 °C. Consequently, to overcome the day/night time lag problem described in Section 1, the thermal storage capacity of the ceiling panels had to accommodate the heat gains within the space during the daily cycle. Standard use profiles for office buildings (e.g. as described in [13]) and data on typical facade constructions with large areas of glazing were used to estimate the following heat gains inside the building in relation to floor area:

High internal thermal loads, open-plan office (Wh/m^2 day)	130
Solar gains in summer (Wh/m^2 day)	190
Total (Wh/m^2 day)	320

To simplify the specification of boundary conditions for the laboratory tests while simulating real conditions, an 8 h exposure time to the full thermal load was assumed. Given a thermal storage capacity of 320 Wh/(m^2 day), a mean heat load of 40 W/m^2 was required.

6.2. Simulation calculations for specification of required ceiling panel properties

Simulation calculations were performed to determine the required ceiling panel characteristics, based on the properties of the basic materials. Key parameters included the thickness of the PCM/gypsum composite layer, the proportion of paraffin and the minimum requirements placed on the PCM in terms of melting range and latent heat of fusion (see Fig. 1).

The design process focused on an office environment with the characteristics specified in the previous section. The following conclusions were drawn from the simulation calculations:

An overall panel thickness of 5 cm is required to store the total heat gain of 320 Wh/m^2 day. The quantity of PCM in the gypsum must be at least 25% by weight.

In order to meet the required temperature boundary conditions, it is important for the melting range of the paraffin to be carefully adjusted to the specific situation. The region

Table 6
Building data and boundary conditions for building simulation

Building	
Facade orientation	West-south-west
Glazed area (m^2)	8
Thermal transmittance (U), glazing (W/m^2K)	0.7
Solar heat gain coefficient (SHGC), glazing	0.5
Solar heat gain coefficient (SHGC), glazing with solar control	0.05
Floor area (m^2)	24
Concrete floor/slab thickness (cm)	25
Maximum internal heat load (W/m^2)	18
Thermally activated ceiling system	
PCM ceiling panel thickness (cm)	5
Percentage PCM in ceiling panel (% by weight)	25
Capillary tube internal/external diameter (mm)	2/3
Tube spacing (cm)	3
Flow temperature (°C)	18
Specific water mass flow rate in relation to ceiling area (kg/hm^2)	15
Operating time for recooling (h)	22:00–06:00

with maximum values of specific heat must therefore correspond to 21–22 °C.

To avoid large temperature gradients inside the material, the ceiling panels must exhibit good thermal conductivity over the entire cross-section. Here, the simulation calculations showed a mean target value of $\lambda = 1.2$ W/mK to be practicable.

6.3. Building-integrated simulation calculations

To check that ceiling panels with the above properties would perform satisfactorily under real load and weather conditions, computational simulations were carried out using building-integrated ceiling modules. The building data and boundary conditions selected for the computations are summarized in Table 6. The assumed environment (building use) is one with high internal thermal loads plus high solar gains due to the almost fully glazed facade.

As the graph in Fig. 10 shows, the thermally activated ceiling system ensures that the room temperature remains within a comfortable range even when outdoor temperatures are high. The mean ceiling temperature also indicates that the melting range of the paraffin is fully exploited.

For reasons of comparison the same building was calculated without PCM ceiling panels. Thereby the conventional piping system was assumed to be placed in the center of the slab and a sheet steel panel as suspended ceiling guaranteed equal boundary conditions like in the case with PCM. From the corresponding curve it can be seen that with this classical tabs-setup in conjunction with a suspended ceiling significantly higher temperatures would arise than with the PCM system.

7. Experimental study

7.1. Production of prototypes

The results from the design process were used to produce prototype modules for the laboratory tests. As values of approx. 0.8–1.0 W/mK are quoted in background literature for the thermal conductivity of gypsum, no preliminary measures were implemented to increase the thermal conductivity of the unit. However, conductivity readings from the first prototype indicated a value as low as 0.2 W/mK—a result of the higher porosity of the gypsum/PCM composite compared to normal gypsum. To achieve the necessary increase in conductivity by a factor 6, aluminum fins were incorporated in the ceiling element. Theoretical estimates put the required spacing at around 3 cm, with fins extending across the full cross-section. The assembly selected for the prototype is shown in Fig. 11. The effectiveness of the measure

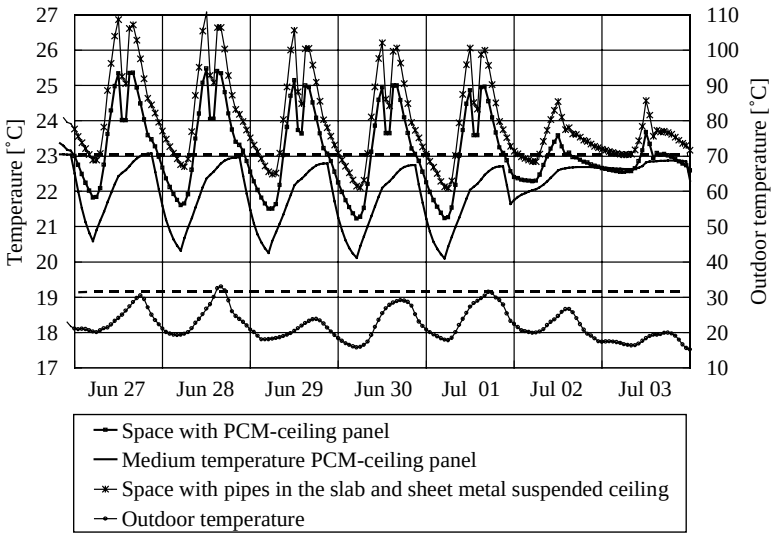

Fig. 10. Temperature profiles in real environment with integrated ceiling panels during summer week.

Fig. 11. Aluminum fins to increase the conductivity in the PCM/ Gyp- sum-composit.

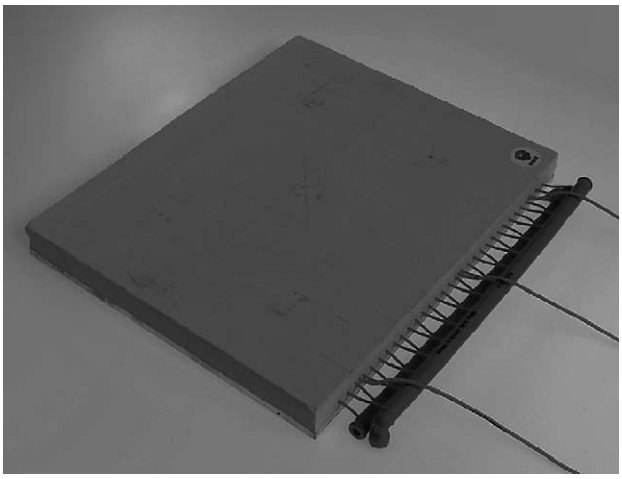

Fig. 12. Prototype of 0.25 m^2 ceiling panel for laboratory test.

was confirmed by the laboratory tests, which recorded values of 1.1–1.2 W/mK.

The initial paraffin mix used as PCM comprised hexadecane and octadecane. First tests showed the melting curve to be some 3 K too high. The new heptadecane-based paraffin mix subsequently produced and encapsulated proved to be ideal in terms of temperature distribution for the following tests.

Fig. 12 shows a complete ceiling panel prior to mounting in the test stand. The capillary tube system cast into the composite is clearly visible in the foreground.

7.2. Design of laboratory tests

The aim of the laboratory tests was to verify the performance of the system prototypes following their optimization in the simulation process. The test set-up shown in Fig. 13 served to provide a realistic simulation of the processes occurring in both room and ceiling panel. The hot box tests were designed to allow cyclical heating and cooling of the ceiling panels and collection of data on temperature conditions and energy storage capacity.

An electrical heating plate (a) was used to simulate the environmental thermal loads. The adjacent neoprene layer (b) has a thermal resistance of 0.1 m^2K/W, equivalent to a realistic combined heat transfer coefficient between the room temperature and the surface temperature of approx. 10 W/m^2K. The temperature measured on the heating plate (c) was therefore, roughly equivalent to the corresponding room temperature. Additional temperature sensors were used to measure the mean surface temperatures on the lower (d), and upper faces (e) of the panel. Circulation of cold water through the capillary tube system (f) allowed the ceiling panel to be recooled after a heating cycle.

7.3. Performance of laboratory tests

Fig. 14 shows a measurement cycle for the optimized ceiling panel. The PCM accounts for some 23% by weight of the ceiling panel, equivalent to a PCM mass of approx. 13 kg/m^2 ceiling area. The ceiling panel was subjected to a constant heat load of approx. 40 W/m^2. The graph shows the temperature curves for the room-side (d) and rear (e) ceiling panel surfaces as well as the temperature measured

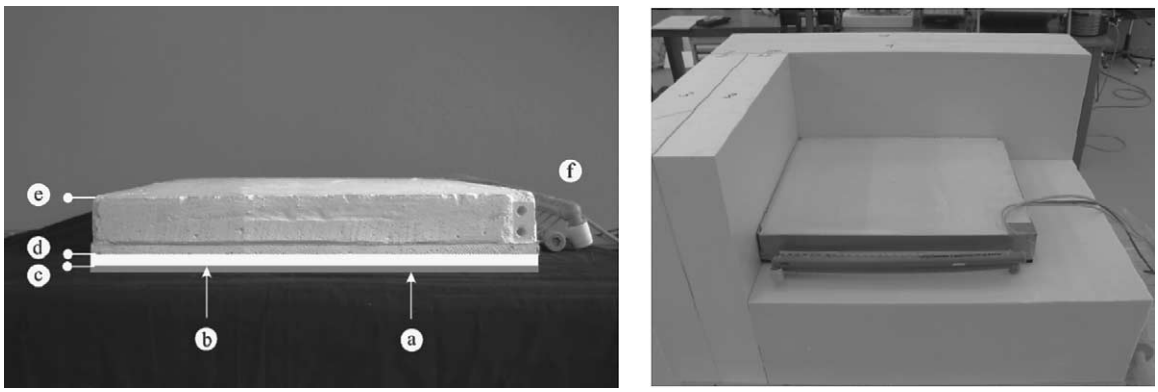

Fig. 13. Laboratory test set-up with prototype ceiling panel.

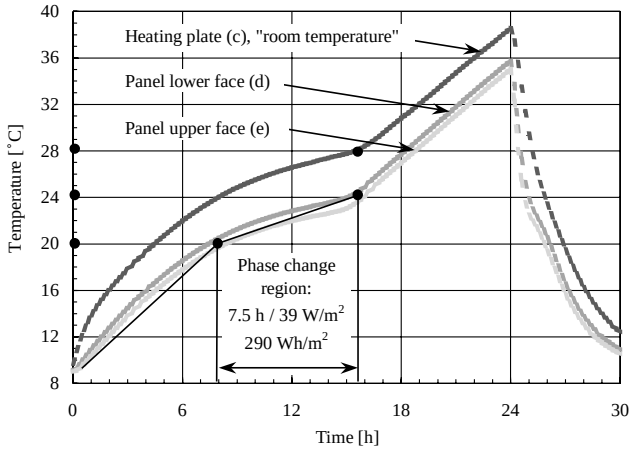

Fig. 14. Temperature profiles for test cycle recorded in laboratory.

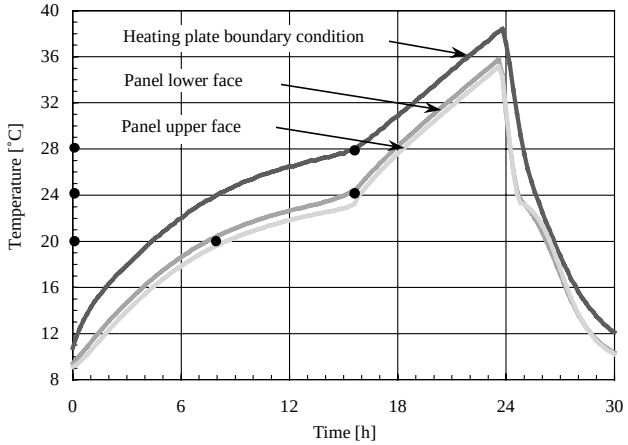

Fig. 15. Temperature profiles for test cycle calculated with model.

between heating plate and neoprene (c), equivalent to the corresponding room temperature.

The phase change process undergone by the PCM in the ceiling panel is clearly reflected by the leveling off of the heating curves after 8 h. The required operating range in the real application is limited to this phase change region as the energy storage here slows down the rise in temperature. In this particular case, subject to an average load of 39 W/m^2, the melting process lasted for 7.5 h, during which a total of 290 Wh/m^2 thermal energy was stored. That the storage capacity fell short of the projected 320 Wh/m^2 is due to the lower absolute quantity of paraffin incorporated in the panel, as dictated by the ultimate porosity and, hence, density of the composite—properties not fully controllable during the mixing and filling process.

The fact that phase change commences at 20 °C confirms that the paraffin's melting range was ideally adjusted to requirements. The paraffin contained in the ceiling panel, is therefore, completely solid at the start of the daily cycle, allowing its full storage capacity to be exploited.

At the end of phase change, the panel temperature is up by 4 K to 24 °C. During this period, the (virtual) room temperature rises to approx. 28 °C. A continued supply of energy subsequently triggers a sharper temperature increase as all the paraffin is now in a liquid state with a correspondingly lower specific heat capacity. Due to the low thermal capacity (product of density and specific heat capacity), the performance of the PCM system outside the operating (melting) range is therefore more critical than that of heavily constructed buildings with solid elements. This factor warrants particular attention in the design of PCM based thermally activated wall and ceiling systems.

A simulation calculation using boundary conditions transferred from the laboratory test to the model yielded the results shown in Fig. 15. The fact that these largely agree with the measured values is further proof of the model's accuracy in simulating the thermal behavior of the ceiling panels.

8. Application

8.1. Prototype building

Following verification in laboratory tests and simulation calculations of the panel's thermal performance, detail design work commenced on the pilot application for the new-build administrative facility of BASF AG's housing company "Ludwigshafener Wohnungsunternehmen LUWOGE/GEWOGE" (Fig. 16). This primarily entailed the detailing and production of units (Fig. 17) for incorporation in the ceiling of the 200 m^2 exhibition hall.

The pilot system is scheduled for launch in June 2003. A separate monitoring project will be implemented as of this date to further check the practicability of the concept.

The combustibility of paraffin and its high fire load may negatively impact the development of any fire in the

Fig. 16. Interior of new-build administrative facility of the "Ludwigshafener Wohnungsunternehmen LUWOGE/GEWOGE".

Fig. 17. Open ceiling module for pilot building prior to pouring composite.

building. However, given the envisaged use of the space and the provision of a sprinkler system, the ceiling system fitted in the LUWOGE/GEWOGE pilot building meets current German fire regulations with a B1 fire-resistance rating.

9. Conclusions and outlook

A prerequisite for the use of renewable energy sources, e.g. cool night air, for cooling of office buildings is the provision of a suitable storage system capable of accommodating the thermal loads arising within the room during the daytime. This study describes the development of such a system in the form of a thermally activated ceiling panel. As alteration and refurbishment schemes look set to account for an increasing proportion of construction work, the focus was on minimizing overall panel thickness while providing ample storage capacity. It was demonstrated, by means of simulation calculations and laboratory tests, that a 5 cm layer of microencapsulated PCM (25% by weight) and gypsum suffice to maintain a comfortable room temperature in standard office buildings.

The system's features also make it ideal for use in lightweight structures, the incorporation of additional thermal mass offering an efficient means of moderating temperature amplitudes in this type of building.

While the micro-encapsulation of the PCM, its bedding in gypsum and encasement in a sheet steel tray ensure a certain level of fire resistance, further improvements are needed with regard to fire protection to broaden the system's applicability. A follow-up project will therefore be implemented to assess suitable fire precautions to be investigated in fire tests.

Acknowledgements

This project was funded partly by the Swiss Federal Laboratories for Materials Testing and Research (EMPA) and partly by TRANSSOLAR Energietechnik GmbH. We gratefully acknowledge the particularly valuable discussions with Dr. Ekkehard Jahns of BASF and with Stefan Holst and Christian Matt of TRANSSOLAR.

References

[1] M. Koschenz, B. Lehmann, Thermoaktive Bauteilsysteme tabs, EMPA, Duebendorf Switzerland, ISBN 3-905594-19-6, 2000 (German only).
[2] P. Schossig et al., Mikroverkapselte Phasenwechselmaterialien in Wandverbundsystemen zur Komfortsteigerung und Energieeinsparung, Frauenhofer-Institut für Solare Energiesysteme ISE, Freiburg Germany, 2001.
[3] Projektinfo 06/2002, Latentwärmespeicher in Baustoffen, BINE Informationsdienst, Karlsruhe, Germany, 2002.
[4] TRNSYS 15, Transient System Simulation Program, Solar Energy Laboratory (SEL), University of Wisconsin, Madison, USA, 2000.
[5] G.A. Lane, Solar Heat Storage: Latent Heat Materials, CRC Press, Boca Raton, Florida, ISBN 0-8493-6585-6, 1983.
[6] E. Jahns, Microencapsulated Phase Change Material, IEA Annex 10, fourth Workshop, Bendiktbeuern Germany, 1999.
[7] P.W. Egolf, H. Manz, Theory and modeling of phase change materials with and without mushy regions, Int. J. Heat Mass Transfer, 37 (18) (1994) 2917–2924.
[8] P.W. Egolf, M. Koschenz, B. Lehmann, Latentwärmespeicher für die Sonnenenergienutzung: Lade- und Entladevorgänge, Schlussbericht NEFF 515, 1997 (German only).
[9] S.V. Patankar, Numerical Heat Transfer and Fluid Flow, Hemisphere Publishing Corporation, Washington, 1980.
[10] M. Minkowycz, E.M. Sparrow, G.E. Schneider, R.H. Pletcher, Handbook of Numerical Heat Transfer, Wiley-Interscience, New York, 1988, pp. 522–526.
[11] S. V. Patankar, B. R. Baliga, A new finite-difference scheme for parabolic differential equations, Numerical Heat Transfer, 1 (1978) 27.
[12] V. Alexides, A. D. Solomon, Mathematical Modeling of Melting and Freezing Processes, Hemisphere Publishing Corporation, Washington, 1993, p. 47.
[13] SWKI Richtlinie 95-3: Jährlicher Energiebedarf von lüftungstechnischen Anlagen, Swiss Association of HVAC Engineers, Berne, Switzerland, 1997.